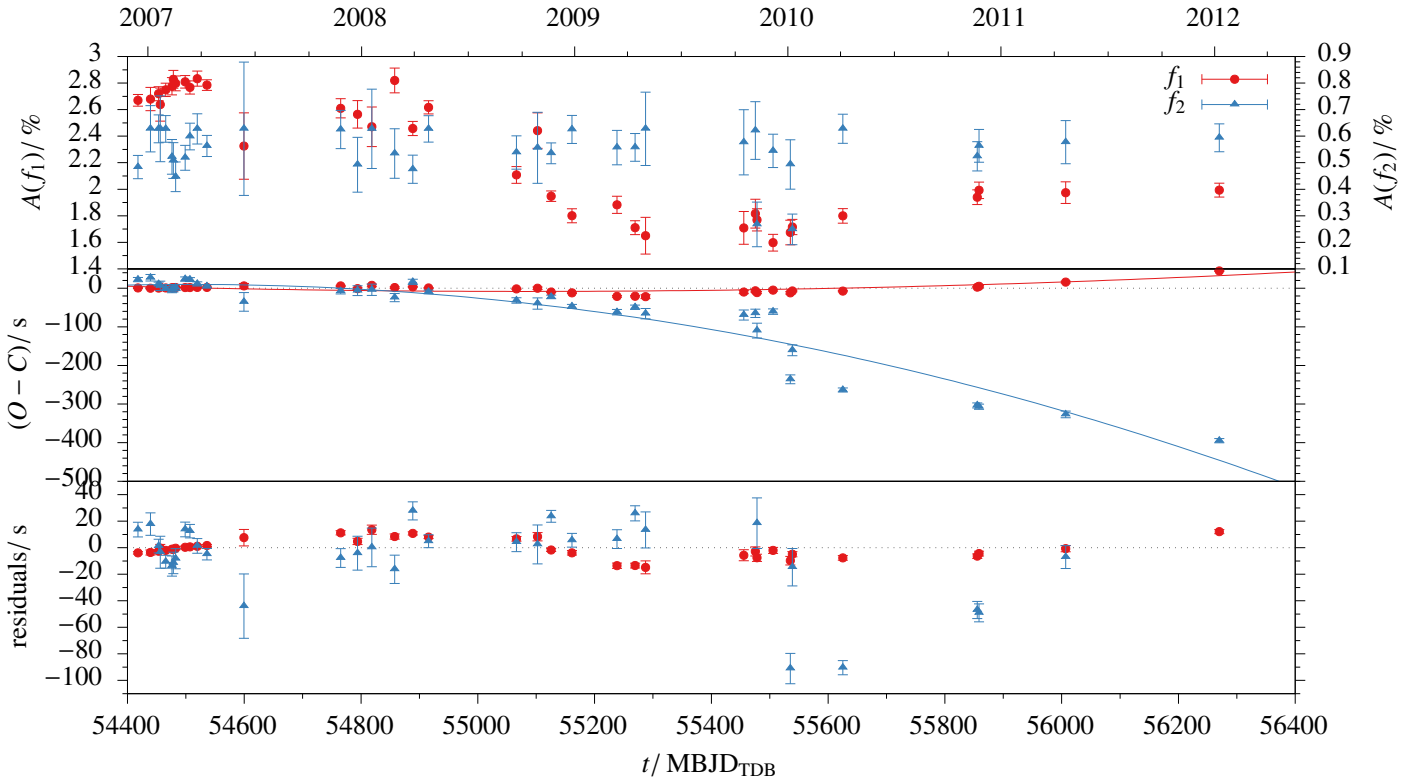

Fig. 8. Results for the two main pulsations of DW Lyn. *Top panel*: amplitudes. *Middle panel*: fits of the O–C data with second order polynomials in time. *Lower panel*: residuals.

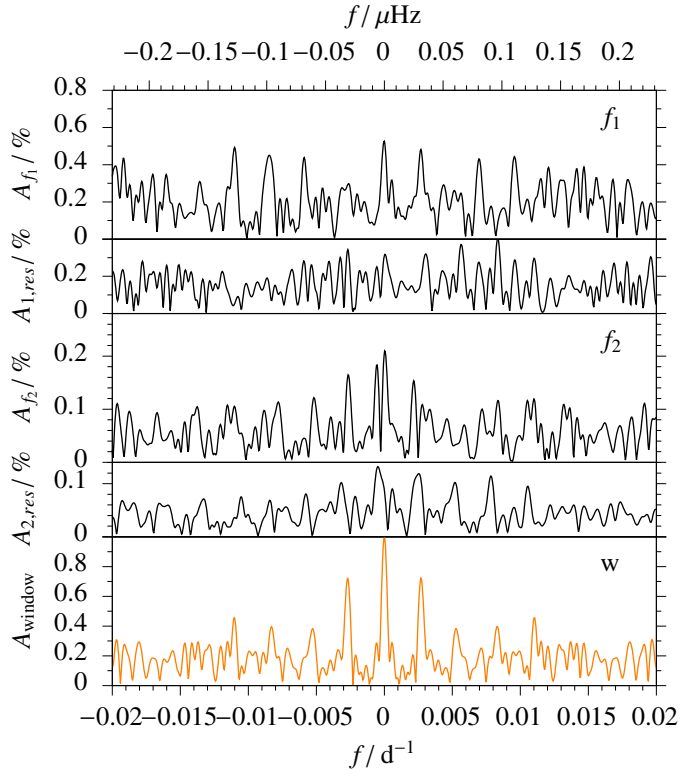

Fig. 9. Amplitude spectrum of V1636 Ori of the main pulsation frequency $f_1 = 631.7346\,\mathrm{d}^{-1}$ (*top*), $f_2 = 509.9780\,\mathrm{d}^{-1}$ (*middle*) with the respective residuals after the pre-whitening below and the normalised window-function (*bottom*).

$f_3 = 642.0516\,\mathrm{d}^{-1}$ are presented next to f_1 in Fig. 11. Another peak at about $665\,\mathrm{d}^{-1}$ consists of at least two frequencies at $664.488549\,\mathrm{d}^{-1}$ and $665.478133\,\mathrm{d}^{-1}$, but they are not sufficiently resolvable within the individual epochs, and lead to uncertainties in the O–C analysis that are too large.

Figure 12 shows the resulting O–C diagram and the amplitudes at different epochs. Due to the large observational gap from 2003 to 2008 with only one block of observations in between, we had difficulties avoiding errors in cycle count. In order to avoid a phase jump, we increased the averaging window for initial phase values to $q = 6$. With this set up, the changes in pulsation frequencies read as follows: $\dot{P}/P_{f1} = (1.7 \pm 1.6) \times 10^{-7}\,\mathrm{d}^{-1}$, $\dot{P}/P_{f2} = (2.4 \pm 0.4) \times 10^{-5}\,\mathrm{d}^{-1}$ and $\dot{P}/P_{f3} = (4.0 \pm 0.5) \times 10^{-6}\,\mathrm{d}^{-1}$. While f_2 and f_3 show no significant variation of pulsation amplitude, f_1 varies by 1.5 per cent (amplitude) or 50 per cent (relative). Thus, the corresponding phase changes should be interpreted with caution. Charpinet et al. (2006) identified the radial order k and degree l from asteroseismic modelling to be f_1: $l = 2, k = 2$; f_2: $l = 4, k = 1$; f_3: $l = 3, k = 2$. These combinations do not allow a direct comparison of our $\dot{P}$ measurements to the model calculations from Charpinet et al. (2002), but the sign of $\dot{P}$ indicates QQ Vir to be in the stage of He burning.

4.4. V541 Hya

The amplitude spectrum in Fig. B.4 shows two pulsation modes with frequencies at $f_1 = 635.32218\,\mathrm{d}^{-1}$ and at $f_2 = 571.28556\,\mathrm{d}^{-1}$. Both of them show a complex behaviour (Fig. 13), indicating unresolved multiplets and/or frequency changes that we see also in the O–C diagrams (Fig. 14). The

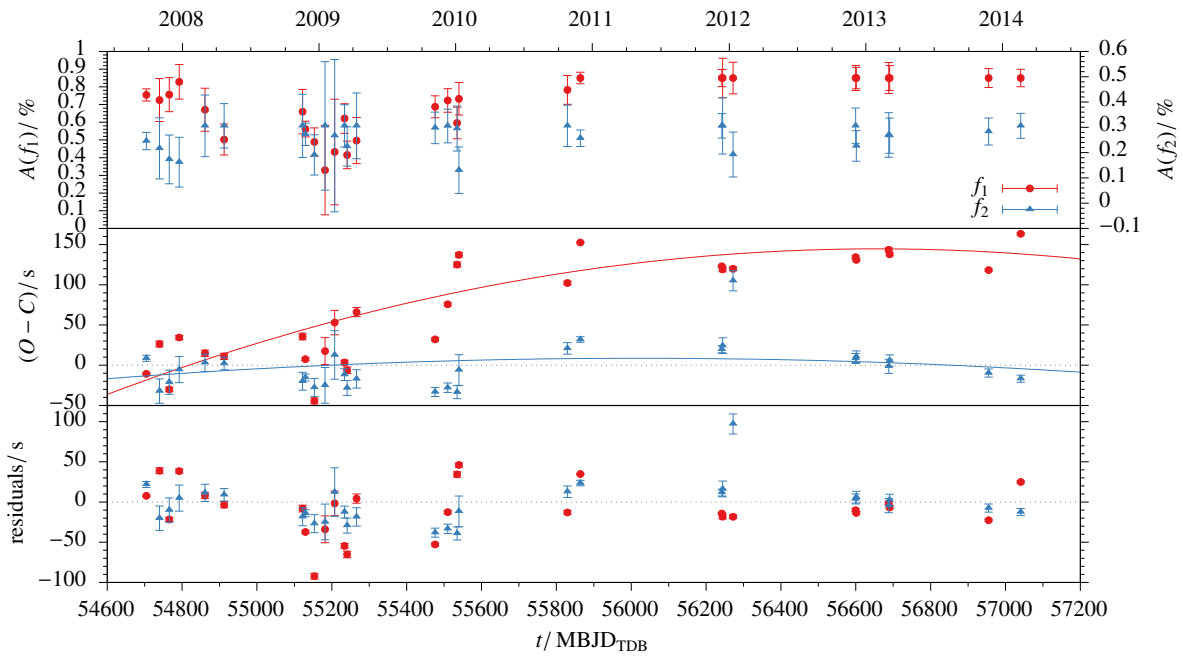

Fig. 10. Results for the two main pulsations of V1636 Ori. *Top panel*: amplitudes. *Middle panel*: fits of the O–C data with second order polynomials in time. *Lower panel*: residuals.

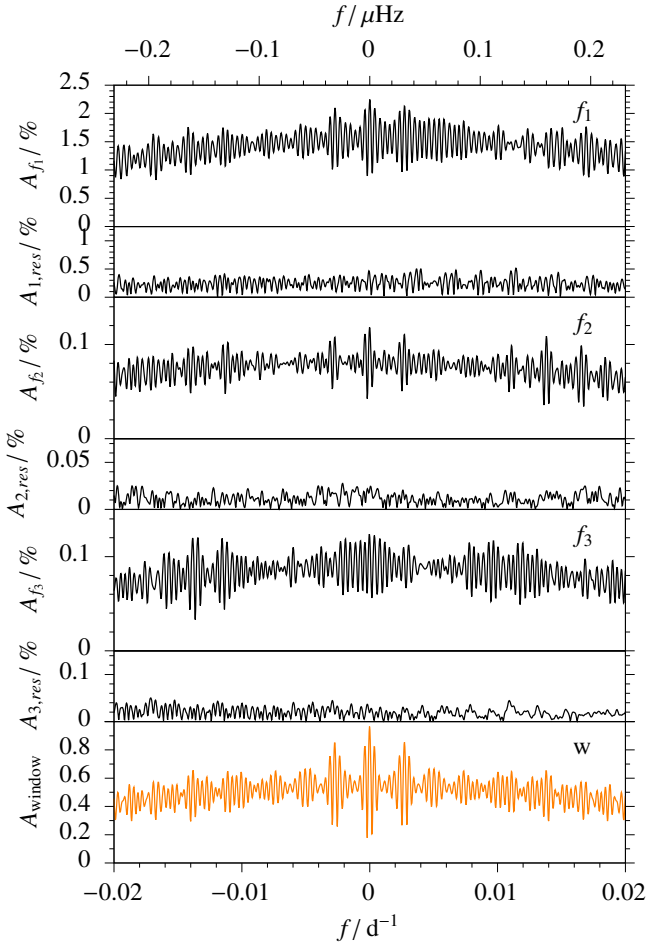

Fig. 11. Amplitude spectrum of QQ Vir of the main pulsation frequency $f_1 = 626.877628\,\mathrm{d}^{-1}$ (*top*), $f_2 = 552.00713\,\mathrm{d}^{-1}$ (*top middle*), $f_3 = 642.0516\,\mathrm{d}^{-1}$ (*bottom middle*) with the respective residuals after the pre-whitening below and the normalised window-function (*bottom*).

S/N for a third frequency at $603.88741\,\mathrm{d}^{-1}$ is not sufficient for the O–C analysis. Similar to V1636 Ori, the amplitude spectrum obtained from the TESS light curve in Fig. A.2 shows no evidence for g-mode pulsations with amplitudes greater than 0.4 per cent.

Randall et al. (2009) speculated about rotational mode splitting for f_3 with $\Delta f_{3,-} = 5.12\,\mu$Hz and $\Delta f_{3,+} = 3.68\,\mu$Hz. The asteroseismic modelling associates f_1 with a $l = 0$ mode and f_2 with $l = 0$ or 1 mode (depending on the favoured model). f_3 corresponds to a $l = 2$ mode. They caution this interpretation due to their limited resolution in frequency space, the mode splitting could be an unresolved quintuplet. Our data set shows no clear evidence for a mode splitting with $\Delta f_{3,-} = 5.12\,\mu$Hz or $\Delta f_{3,+} = 3.68\,\mu$Hz (see Fig. 15) but rather a mode splitting for f_1 and f_2 with about $\Delta f = 0.08\,\mu$Hz (Fig. 13). Assuming these modes are of degree $l = 1$, this could be interpreted as a triplet. But Randall et al. (2009) model these modes with a degree of $l = 0$, which does not support a mode splitting into triplets.

The O–C diagram in Fig. 14 shows the analysis of the two main pulsation modes and the variation of the pulsation amplitudes. The second order fits in time correspond to changes in period of $\dot{P}/P_{f1} = (-1.49 \pm 0.11) \times 10^{-5}\,\mathrm{d}^{-1}$ and $\dot{P}/P_{f2} = (-0.7 \pm 1.5) \times 10^{-5}\,\mathrm{d}^{-1}$. For f_2, the change in period does not significantly differ from the null hypothesis. Assuming these changes origin from stellar evolution, V541 Hya might just have passed the point of sign change in $\dot{P}$ and at the beginning of the contraction phase. While the arrival times scatter widely, the amplitudes of both pulsations remain almost constant within the uncertainties. If V541 Hya is in its evolution close to starting the contraction phase, as indicated by a $\dot{P}$ close to zero, the changes in stellar structure may cancel the strict phase coherence.

4.5. Testing the sub-stellar companion hypothesis

In order to set upper limits to the mass of a companion, we computed a series of synthetic O–C curves for different orbital

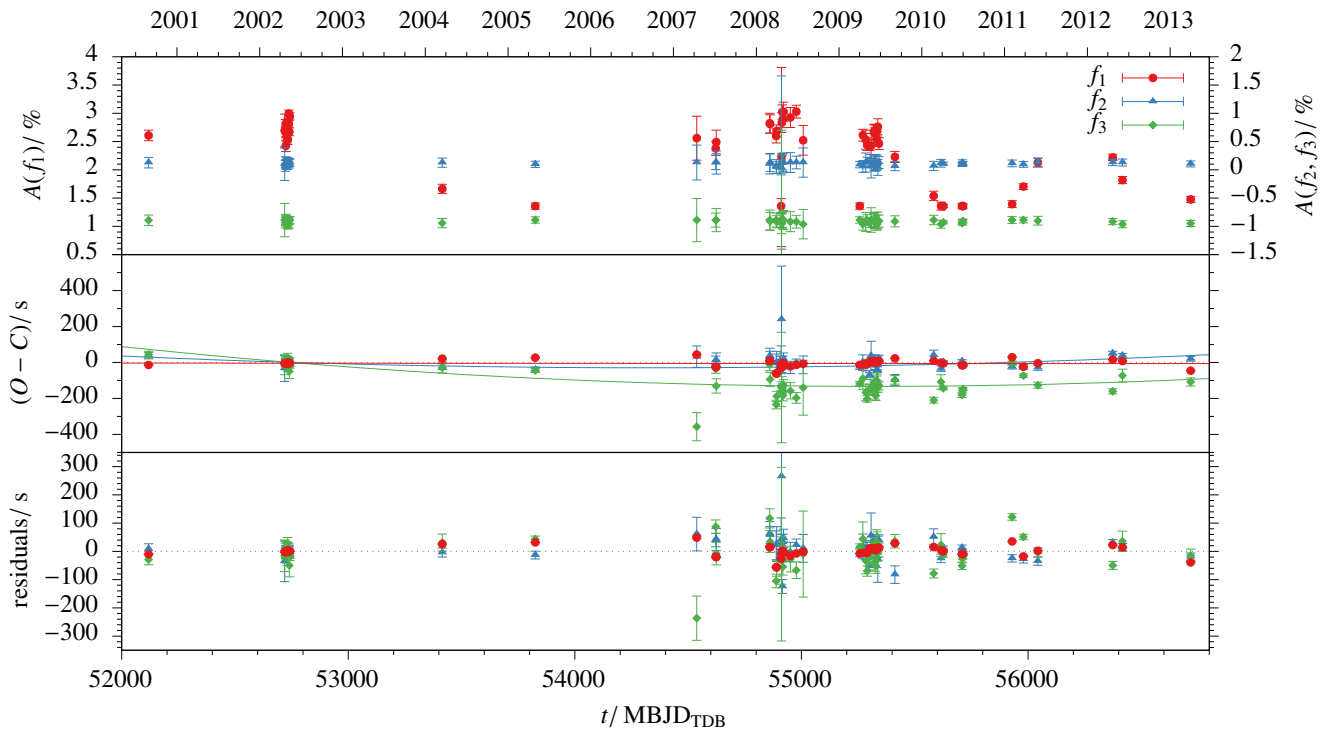

Fig. 12. Results for the three main pulsations of QQ Vir. *Top panel*: amplitudes. f_3 has a vertical offset of −1 for clarity. *Middle panel*: fits of the O–C data with second order polynomials in time. *Lower panel*: residuals.

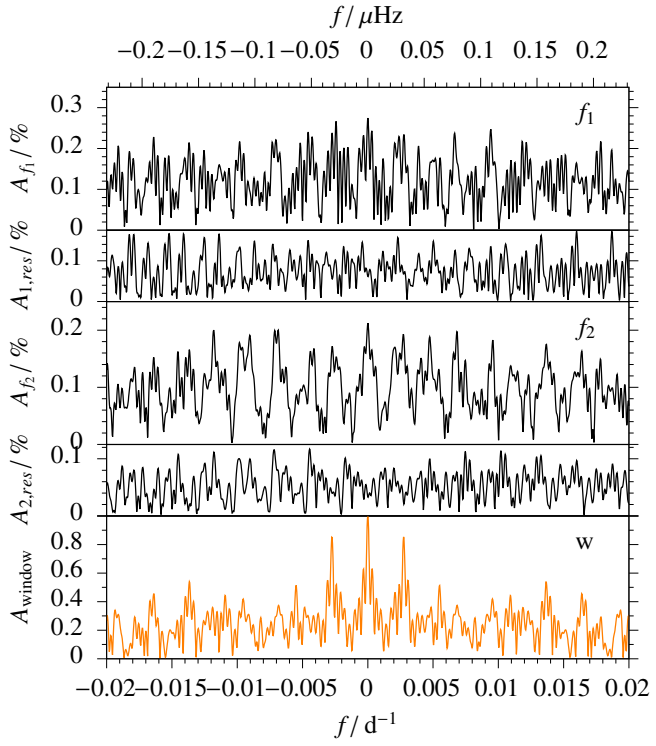

Fig. 13. Amplitude spectrum of V541 Hya of the main pulsation frequency $f_1 = 635.32218\,\mathrm{d}^{-1}$ (*top*), $f_2 = 571.28556\,\mathrm{d}^{-1}$ (*middle*) with the respective residuals after the pre-whitening below and the normalised window-function (*bottom*).

periods and companion masses, assuming circular orbits, and compared these curves with the O–C measurements after subtracting the long-term variations.

For each synthetic O–C curve, we selected the phase that gives the best fit to the data using a weighted least squares algorithm. For each observational point, we computed the difference, in absolute value and in σ units (where σ is the O–C error), between O–C and the synthetic value. The greyscale in Figs. 16 and 17 corresponds to the mean value of this difference in σ units, which means that the presence of a companion is indicated by a minimum (bright areas) of this parameter. We see that in V1636 Ori, QQ Vir, and V541 Hya, the mean difference for f_1 is always very high, implying that the data are not compatible with a companion. However, these results are limited by the fact that the O–C diagrams of these stars are "contaminated" by other irregular variations, presumably due to other reasons like non-linear interactions between different pulsation modes, for example, and therefore these constraints to the orbital period and mass of a companion must be taken with some caution. For the f_2 and f_3 measurements, the mean difference to the synthetic data is smaller in sigma units (because of the larger uncertainties) and very uniform. The uncertainties of the O–C measurements are not small enough to favour a set of models in the period-mass parameter space.

For f_1 of DW Lyn, there is a significant minimum at about 1450 d (~4 yr) and ~5 $M_{♃}$[2], which is also well visible in the O–C diagram of Fig. 8. This periodicity is not visible in the second frequency f_2 which, however, has much larger error bars due to the much lower amplitude of f_2 with respect to f_1.

Lutz et al. (2011) described a periodicity at 80 days, detected for f_2. We can recover this signal, however, with a low significance. This would correspond to a light-travel time amplitude of 4 s (for $m \sin i \approx 15\,\mathrm{M}_{♃}$), which is smaller than the 15 s measured by Lutz et al. (2011). Nevertheless, this signal is not confirmed by f_1. Thus, we rule out a companion induced signal in the arrival times due to the lack of simultaneous signals in f_1

[2] 1 $M_{♃}$ (Jupiter mass) = 1.899 × 10^{27} kg.

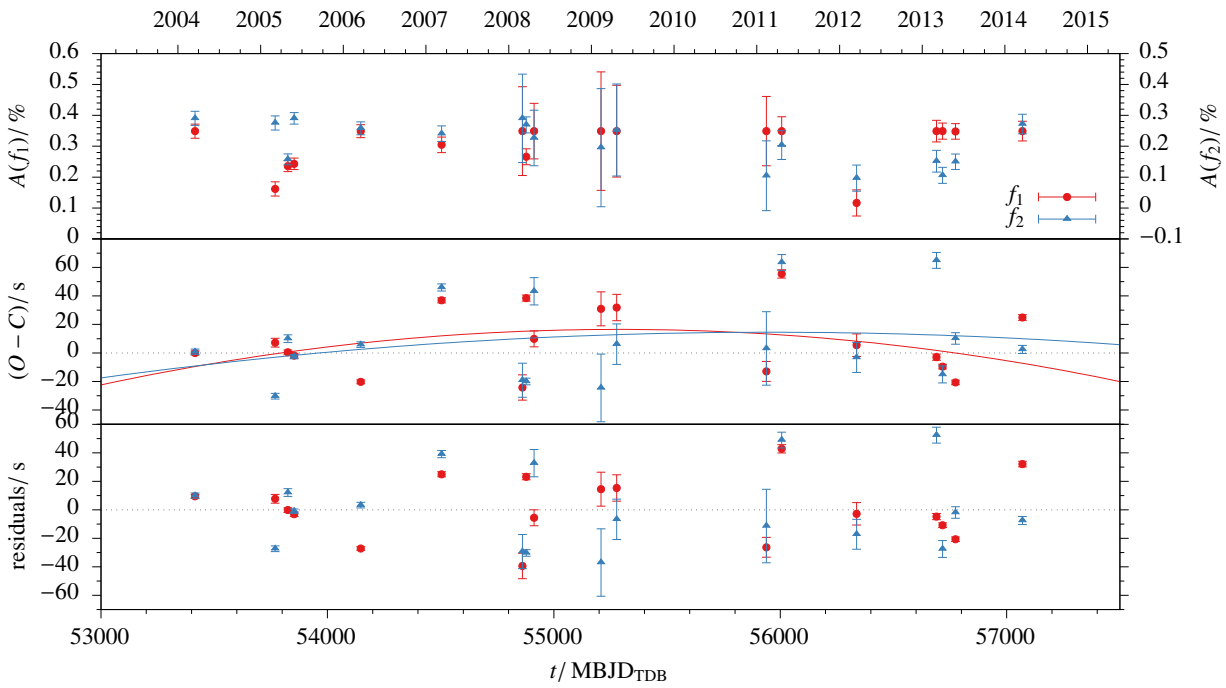

Fig. 14. Results for the two main pulsations of V541 Hya. *Top panel*: amplitudes. *Middle panel*: fits of the O–C data with second order polynomials in time. *Lower panel*: residuals.

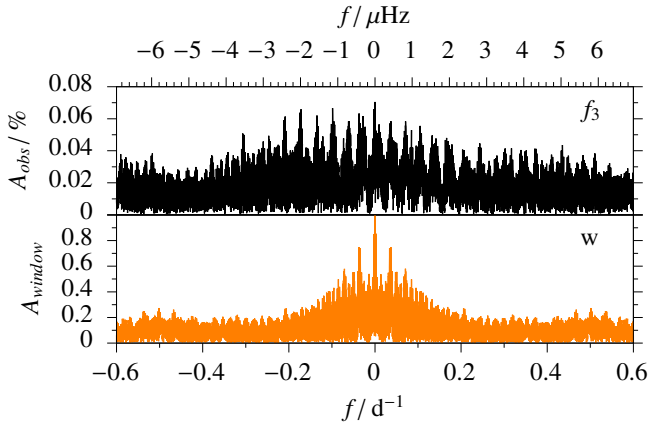

Fig. 15. Amplitude A spectrum with respect to the pulsation frequency $f_3 = 603.88741\,\mathrm{d}^{-1}$ of V541 Hya (*top*) and the normalised window function (*bottom*).

and f_2 with similar amplitude. The tentative signal in f_2 is better explained by mode beating, as already described in Sect. 4.1. The variations seen in the first 200 days of the O–C diagram in Fig. 8 correspond to a periodicity of about 80 days and are accompanied by variations in the amplitude of the pulsation.

For V1636 Ori, Lutz (2011) predicted a period at 160 d and amplitude of 12 s. This can not be confirmed as a companion-induced signal. A periodic signal with an amplitude of 6.5 s (for $m \sin i \approx 15\,M_{♃}$) is indicated in the analysis of f_1, but at a low significance and accompanied by many other signals of similar significance. This periodicity is not confirmed by a significant signal in the measurements of f_2.

5. Summary and conclusion

In this work, we present ground-based multi-site observations for the four sdBs, DW Lyn, V1636 Ori, QQ Vir, and V541 Hya. We investigated variations in the arrival times of their dominant stellar pulsation modes to draw conclusions about secular period drifts and possible sub-stellar companions. All light curves are analysed homogeneously.

From the O–C measurements, we derive an evolutionary timescale from the change in period $\dot{P}$. Comparing to model calculations from Charpinet et al. (2002), we infer the evolutionary phase of the target. Although some $\dot{P}$ measurements are influenced by mode splitting, we can tell from the sign of $\dot{P}_1$ of DW Lyn that the star is likely still in the stage of central He burning. We can draw a similar conclusion from the sign of $\dot{P}$ of QQ Vir. The $\dot{P}$ measurements of V1636 Ori are likely affected by mode splitting, making it difficult to interpret the results in the context of stellar evolution. V541 Hya shows $\dot{P}$ measurements close to zero, which indicates the star being at the transition phase between He burning and contraction due to the depletion of He in the core.

Comparing the atmospheric properties from Table 1 with the evolutionary tracks for different models from Fig. 1 in Charpinet et al. (2002), we can confirm the hypothesis that DW Lyn and QQ Vir are in their He burning phase. V541 Hya agrees within 2σ of the $\log g$ measurement with one model at the turning point between the two evolutionary stages.

However, we can not exclude frequency and amplitude variations on smaller timescales than resolvable by our data set. Using temporally higher resolved *Kepler*-data of KIC 3527751, Zong et al. (2018) cautioned about long-term frequency or phase evolutions ascribing to non-linear amplitude and frequency modulations in pulsating sdBs. We see such effects already in our data set, even with a low temporal resolution compared to the *Kepler* sampling with a duty cycle of more than 90 per cent.

Observations on DW Lyn and V1636 Ori were published by Lutz et al. (2008a, 2011); Schuh et al. (2010); Lutz (2011). Our analysis of these observations, including extended data sets, do not confirm the tentative companion periods of 80 and 160 days,

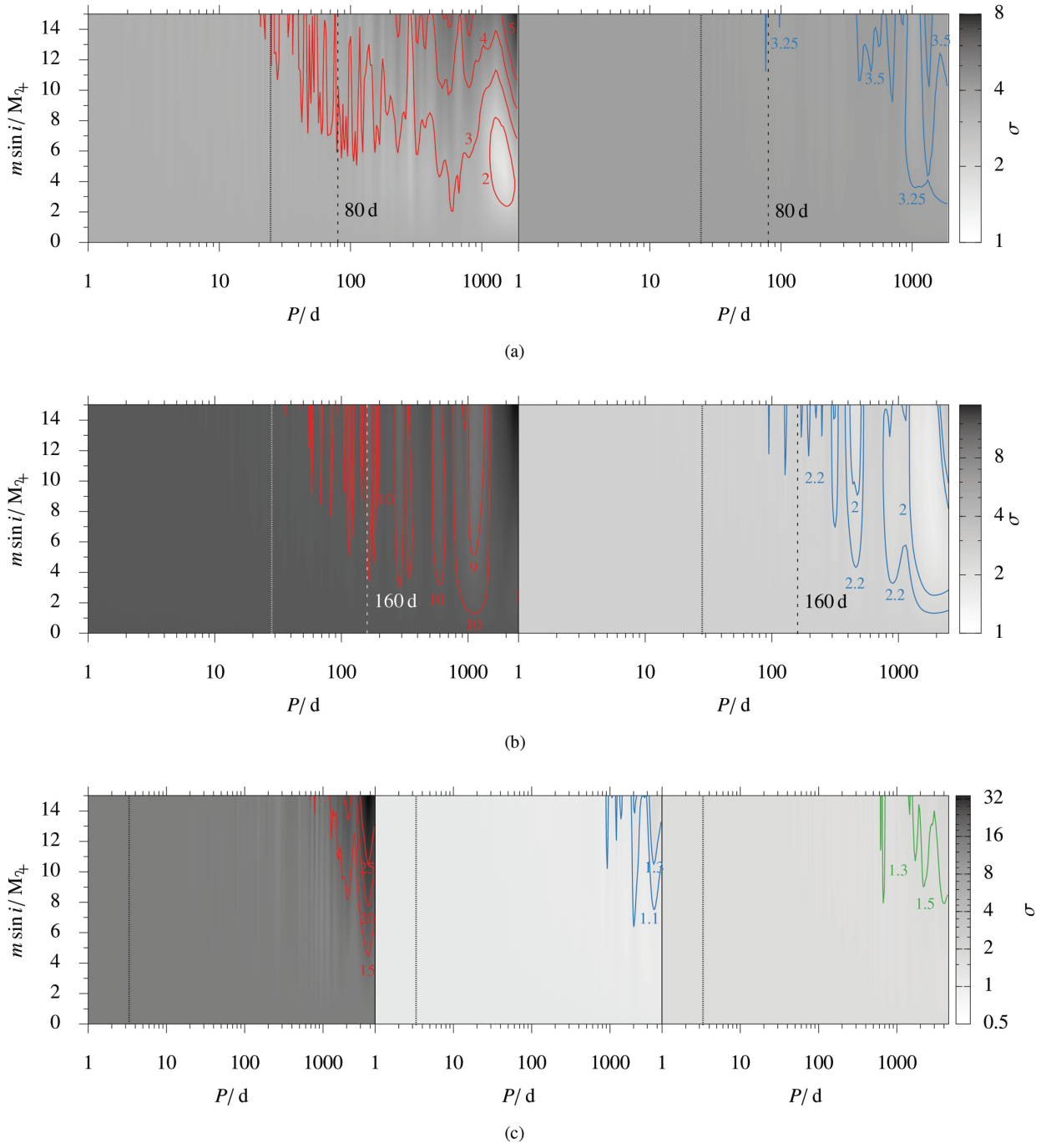

Fig. 16. Minimum companion mass as a function of orbital period. Greyscale shows the difference between the O–C measurements and artificial O–C data generated for a given combination of companion mass and orbit. We note that at this stage, the phase optimisation of the artificial data is done independently for each pulsation frequency. The median of gaps in between the epochs is indicated by a vertical dotted line. See text for more details. (*a*) DW Lyn. Contour lines for f_1 are placed at 2, 3, 4, and 5 σ (*left panel*), and for f_2 at 3.25 and 3.5 σ (*right panel*), as indicated by their labels. The planetary signal proposed by Lutz et al. (2011) at a period of 80 d is indicated as dashed line. (*b*) V1636 Ori. Contour lines for f_1 are placed at 9 and 10 σ (*left panel*), and for f_2 at 2 and 2.2 σ (*right panel*), as indicated by their labels. The planetary signal proposed by Lutz et al. (2011) at a period of 160 d is indicated as dashed line. (*c*) QQ Vir. Contour lines for f_1 are placed at 15, 20, and 25 σ (*left panel*), for f_2 at 1.1 and 1.3 σ (*middle panel*), and for f_3 at 1.3 and 1.5 σ (*right panel*), as indicated by their labels.

respectively. These signals more likely arise due to mode beating indicated by partly unresolved frequency multiplets and amplitude modulations.

Almost all analysed pulsation modes show formal significant changes in arrival times, but the amplitudes of these periodic signals do not correlate with frequencies, excluding the light-travel time effect due to orbital reflex motions for such variations and thus giving upper limits on companion masses. Only DW Lyn might have a planetary companion on a long orbital period, as indicated by one arrival time measurement. But this can not be confirmed with a second measurement, due to larger uncertainties. Additionally, more studies question the presence of already proposed companions, for example, Krzesinski (2015); Hutchens et al. (2017). Our unique sample of long-term observations shows

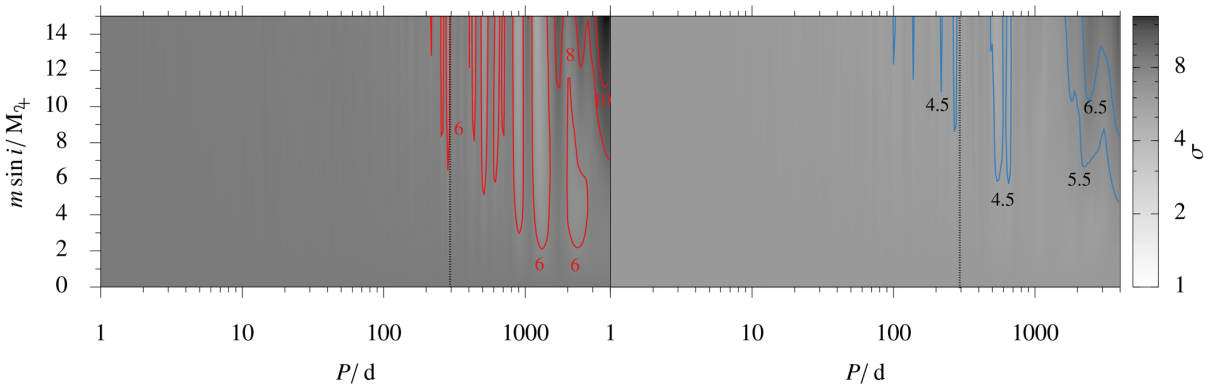

Fig. 17. Continuation of Fig. 16. V541 Hya. Contour lines for f_1 are placed at 6, 8, and 10 σ (*left panel*), and for f_2 at 4.5, 5.5, and 6.5 σ (*right panel*), as indicated by their labels.

a complex behaviour of mode- and amplitude interactions in sdBs which should be addressed in further studies. Until this has been addressed, caution is advised when interpreting O–C pulse arrival times in terms of companions.

Acknowledgements. We thank Wen-Shan Hsiao for observing at the Lulin Observatory and Mike D. Reed for observing at the Baker Observatory and Elia Leibowitz for observing at the WISE observatory. F.M. conducted the work in this paper in the framework of the International Max-Planck Research School (IMPRS) for Solar System Science at the University of Göttingen (Volkswagen Foundation project grant number VWZN3020). D.K. thanks the SAAO for generous allocations of telescope time and the National Research Foundation of South Africa and the University of the Western Cape for financial support. TDO gratefully acknowledges support from the U.S. National Science Foundation grant AST-0807919. L.M. was supported by the Premium Postdoctoral Research Program of the Hungarian Academy of Sciences. This project has been supported by the Lendület Program of the Hungarian Academy of Sciences, project No. LP2018-7/2019. Based on observations made with the Italian Telescopio Nazionale *Galileo* (TNG) operated on the island of La Palma by the Fundación Galileo Galilei of the INAF (Istituto Nazionale di Astrofisica) at the Spanish Observatorio del Roque de los Muchachos of the Instituto de Astrofisica de Canarias. Based on observations collected at the Centro Astronómico Hispánico en Andalucía (CAHA) at Calar Alto, operated jointly by the Andalusian Universities and the Instituto de Astrofísica de Andalucía (CSIC). Based on observations collected at Copernico telescope (Asiago, Italy) of the INAF – Osservatorio Astronomico di Padova. Based on observations made with the Nordic Optical Telescope, operated by the Nordic Optical Telescope Scientific Association at the Observatorio del Roque de los Muchachos, La Palma, Spain, of the Instituto de Astrofisica de Canarias. This paper includes data collected by the TESS mission. Funding for the TESS mission is provided by the NASA Explorer Program.

References

Astropy Collaboration (Robitaille, T. P., et al.) 2013, A&A, 558, A33
Astropy Collaboration (Price-Whelan, A. M., et al.) 2018, AJ, 156, 123
Ballard, S., Fabrycky, D., Fressin, F., et al. 2011, ApJ, 743, 200
Baran, A., Pigulski, A., Kozieł, D., et al. 2005, MNRAS, 360, 737
Baran, A. S., Østensen, R. H., Telting, J. H., et al. 2018, MNRAS, 481, 2721
Barlow, B. N., Dunlap, B. H., & Clemens, J. C. 2011a, ApJ, 737, L2
Barlow, B. N., Dunlap, B. H., Clemens, J. C., et al. 2011b, MNRAS, 414, 3434
Benatti, S., Silvotti, R., Claudi, R. U., et al. 2010, ArXiv e-prints [arXiv:1012.0747]
Bischoff-Kim, A., Provencal, J. L., Bradley, P. A., et al. 2019, ApJ, 871, 13
Blokesz, A., Krzesinski, J., & Kedziora-Chudczer, L. 2019, A&A 627, A86
Bonanno, A., Catalano, S., Frasca, A., Mignemi, G., & Paternò, L. 2003a, A&A, 398, 283
Bonanno, A., Frasca, A., Lanza, A. F., et al. 2003b, Balt. Astron., 12, 287
Charpinet, S., Fontaine, G., Brassard, P., et al. 1997, ApJ, 483, L123
Charpinet, S., Fontaine, G., Brassard, P., & Dorman, B. 2002, ApJS, 140, 469
Charpinet, S., Silvotti, R., Bonanno, A., et al. 2006, A&A, 459, 565
Charpinet, S., Fontaine, G., Brassard, P., et al. 2011, Nature, 480, 496
Charpinet, S., Giammichele, N., Zong, W., et al. 2018, Open Astron., 27, 112
Dreizler, S., Schuh, S. L., Deetjen, J. L., Edelmann, H., & Heber, U. 2002, A&A, 386, 249
Eastman, J., Siverd, R., & Gaudi, B. S. 2010, PASP, 122, 935
Fontaine, G., Brassard, P., Charpinet, S., et al. 2003, ApJ, 597, 518
Green, E. M., Fontaine, G., Reed, M. D., et al. 2003, ApJ, 583, L31
Han, Z., Podsiadlowski, P., Maxted, P. F. L., Marsh, T. R., & Ivanova, N. 2002, MNRAS, 336, 449
Heber, U. 1986, A&A, 155, 33
Heber, U. 2016, PASP, 128, 082001
Hutchens, Z. L., Barlow, B. N., Soto, A. V., et al. 2017, Open Astron., 26, 252
Jones, E., Oliphant, T., & Peterson, P. 2011, SciPy: Open Source Scientific Tools for Python, https://www.scipy.org/
Kilkenny, D. 2010, Ap&SS, 329, 175
Kilkenny, D. 2014, MNRAS, 445, 4247
Kilkenny, D., Koen, C., Stobie, R. S., et al. 1997, Third Conf. Faint Blue Stars (USA: L. David), 77
Kilkenny, D., Stobie, R. S., O'Donoghue, D., et al. 2006, MNRAS, 367, 1603
Krzesinski, J. 2015, A&A, 581, A7
Lee, J. W., Hinse, T. C., Youn, J.-H., & Han, W. 2014, MNRAS, 445, 2331
Lutz, R. 2011, Ph.D. thesis, University of Gottingen, Gottingen, Germany
Lutz, R., Schuh, S., Silvotti, R., et al. 2008a, ASP Conf. Ser., 392, 339
Lutz, R., Schuh, S., Silvotti, R., Kruspe, R., & Dreizler, S. 2008b, Commun. Asteroseismol., 157, 185
Lutz, R., Schuh, S., & Silvotti, R. 2011, AIP Conf. Ser., 1331, 155
Maxted, P. F. L., Heber, U., Marsh, T. R., & North, R. C. 2001, MNRAS, 326, 1391
Murphy, S. J., Bedding, T. R., & Shibahashi, H. 2016, ApJ, 827, L17
Østensen, R., Heber, U., Silvotti, R., et al. 2001, A&A, 378, 466
Østensen, R. H., Reed, M. D., Baran, A. S., & Telting, J. H. 2014, A&A, 564, L14
Otani, T., Oswalt, T. D., Lynas-Gray, A. E., et al. 2018, ApJ, 859, 145
Podsiadlowski, P. 2008, ASP Conf Ser., 401, 63
Postnov, K. A., & Yungelson, L. R. 2014, Liv. Rev. Rel., 17, 60
Provencal, J. L., Montgomery, M. H., Kanaan, A., et al. 2009, ApJ, 693, 564
Qian, S. B., Han, Z. T., Lajús, E. F., et al. 2015, ApJS, 221, 17
Randall, S. K., Van Grootel, V., Fontaine, G., Charpinet, S., & Brassard, P. 2009, A&A, 507, 911
Reed, M. D., O'Toole, S. J., Terndrup, D. M., et al. 2007a, ApJ, 664, 518
Reed, M. D., Terndrup, D. M., Zhou, A.-Y., et al. 2007b, MNRAS, 378, 1049
Ricker, G. R., Winn, J. N., Vanderspek, R., et al. 2015, J. Astron. Teles. Instrum. Sys., 1, 014003
Schaffenroth, V., Barlow, B. N., Drechsel, H., & Dunlap, B. H. 2015, A&A, 576, A123
Schuh, S., Dreizler, S., Deetjen, J. L., Heber, U., & Geckeler, R. D. 2000, Balt. Astron., 9, 395
Schuh, S., Huber, J., Dreizler, S., et al. 2006, A&A, 445, L31
Schuh, S., Silvotti, R., Lutz, R., et al. 2010, Ap&SS, 329, 231
Silvotti, R. 2008, ASP Conf. Ser., 392, 215
Silvotti, R., Østensen, R., Heber, U., et al. 2002, A&A, 383, 239
Silvotti, R., Bonanno, A., Bernabei, S., et al. 2006, A&A, 459, 557
Silvotti, R., Schuh, S., Janulis, R., et al. 2007, Nature, 449, 189
Silvotti, R., Charpinet, S., Green, E., et al. 2014, A&A, 570, A130
Silvotti, R., Schuh, S., Kim, S.-L., et al. 2018, A&A, 611, A85
Stello, D., Arentoft, T., Bedding, T. R., et al. 2006, MNRAS, 373, 1141
Sterken, C. 2005, ASP Conf. Ser., 335, 3
Stumpe, M. C., Smith, J. C., Van Cleve, J. E., et al. 2012, PASP, 124, 985
Telting, J. H., & Østensen, R. H. 2004, A&A, 419, 685
Webbink, R. F. 1984, ApJ, 277, 355
Wolszczan, A., & Frail, D. A. 1992, Nature, 355, 145
Zong, W., Charpinet, S., Fu, J.-N., et al. 2018, ApJ, 853, 98

Appendix A: TESS data

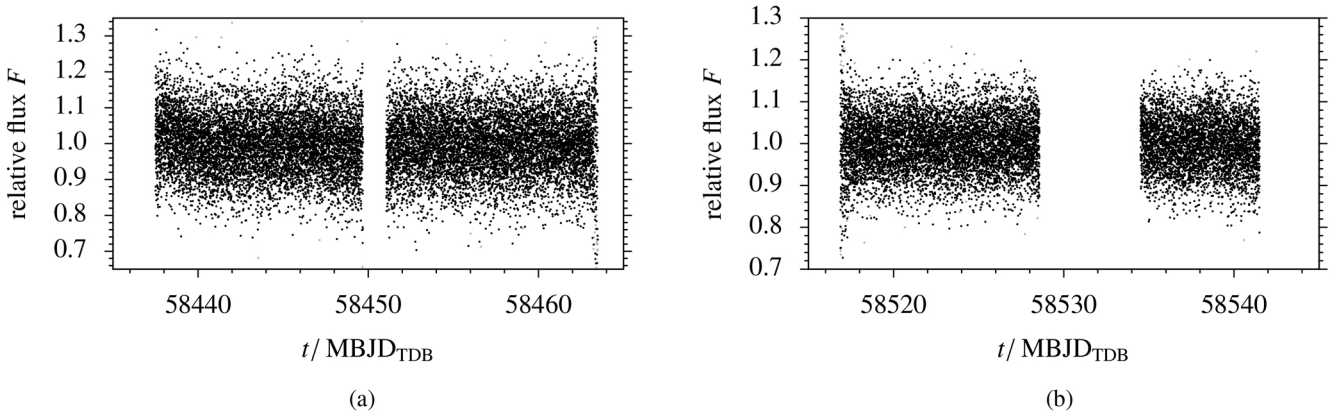

Fig. A.1. Light curves of the TESS observations. Grey points are considered outliers and partially exceeding the plotting range. (*a*) V1636 Ori. (*b*) V541 Hya.

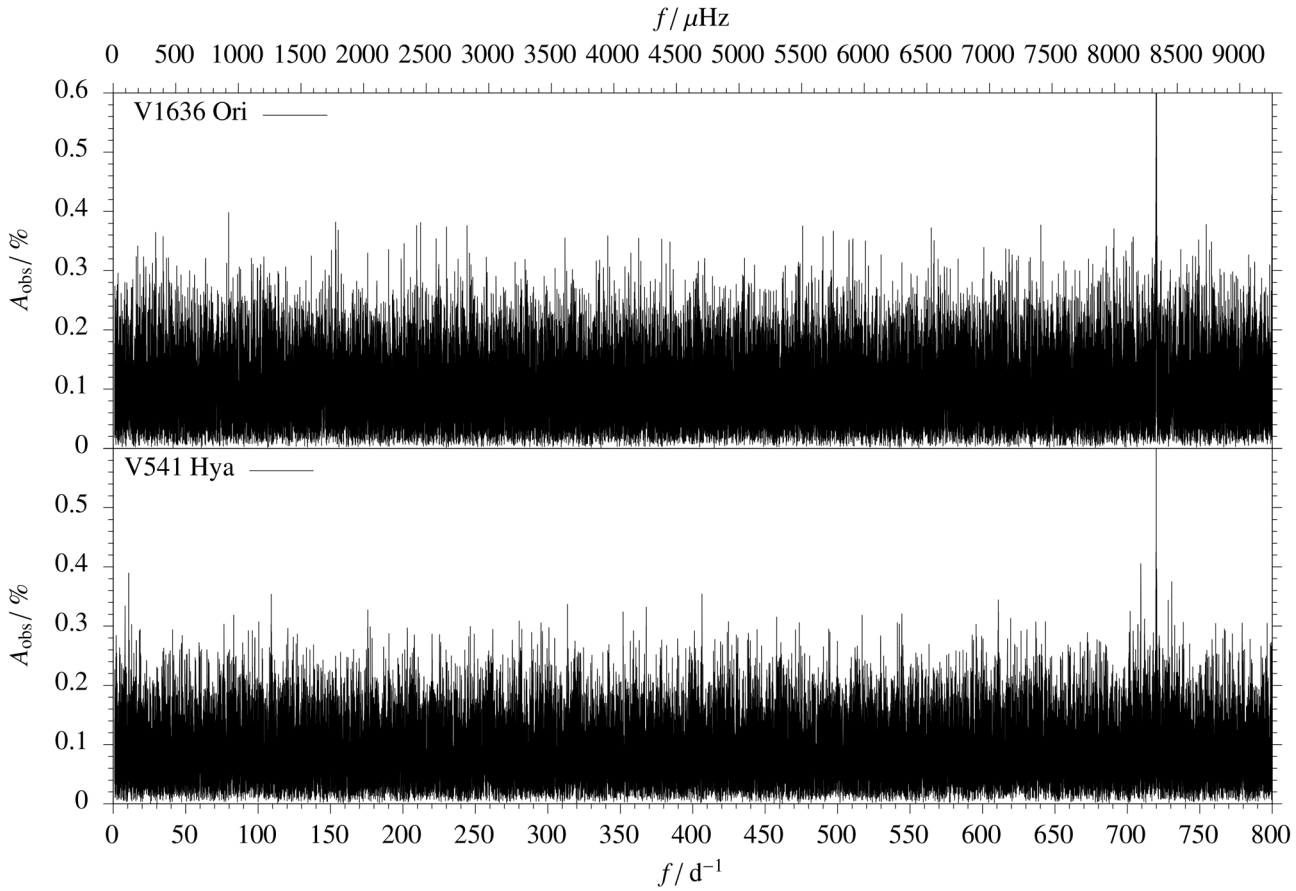

Fig. A.2. Amplitude A spectrum of the TESS observations. *Upper panel*: spectrum of V1636 Ori. *Lower panel*: spectrum of V541 Hya. The only peak above the noise level is the 120 s alias due to the cadence of the observations.

Appendix B: Amplitude spectra

Table B.1. Additional pulsation modes identified for our targets not used in the O–C analysis due to their low S/N.

Target	f/d^{-1}	$A/\%$
DW Lyn	475.8231(2)	0.09(18)
	319.4042(3)	0.06(12)
	463.0100(6)	0.03(18)
V1636 Ori	566.24031(3)	0.6(3)
QQ Vir	733.0704(1)	0.3(1)
	664.4886(1)	0.2(1)
	572.73611(5)	0.19(9)
	664.7122(1)	0.1(1)
	434.1522(6)	0.01(7)
	502.410(2)	0.01(9)
V541 Hya	531.16759(16)	0.03(7)
	603.88741(6)	0.03(8)

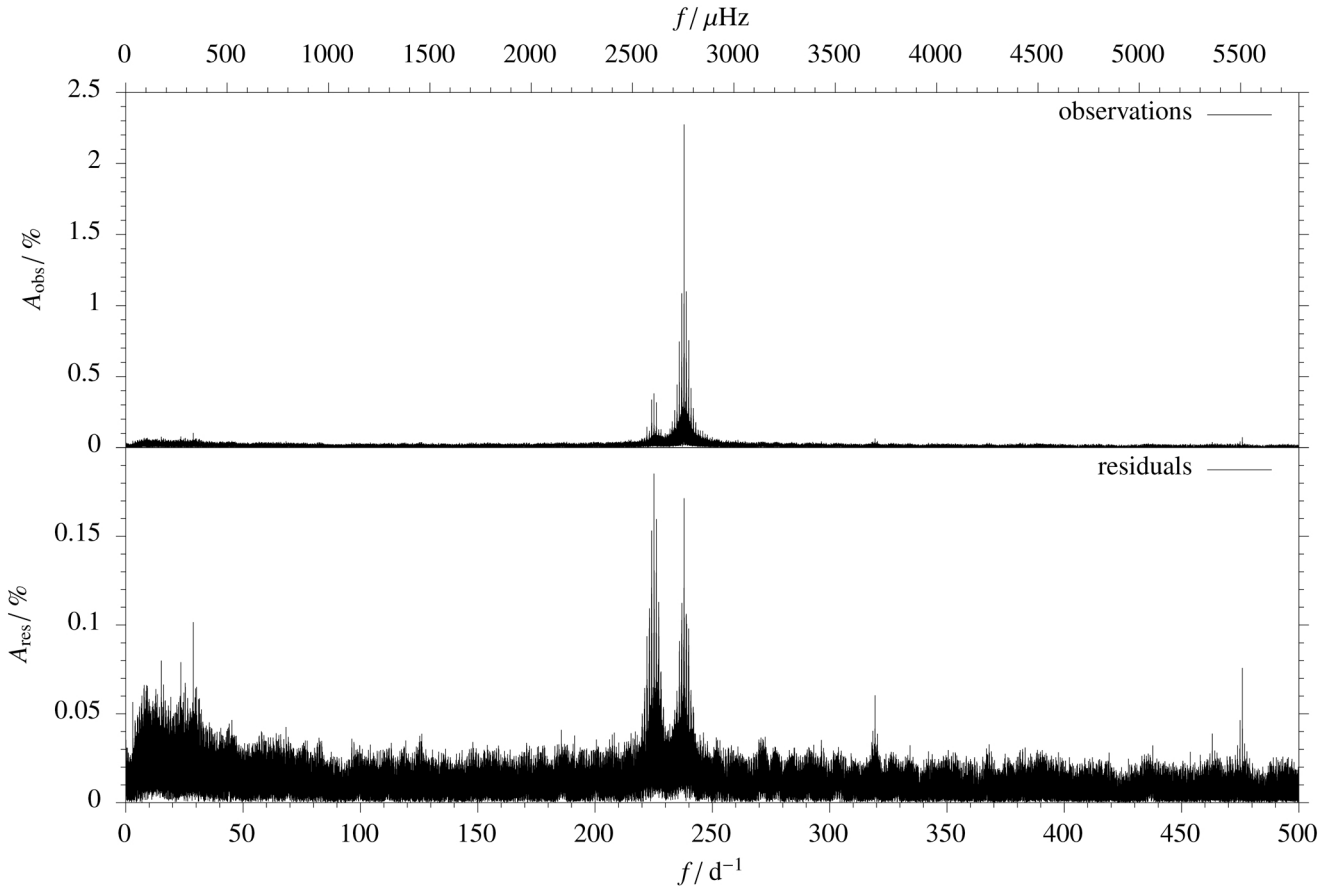

Fig. B.1. Amplitude spectrum of DW Lyn. *Upper panel*: observations $A_{\rm obs}$. *Lower panel*: residuals $A_{\rm res}$ after subtracting the light curve models from the observations.

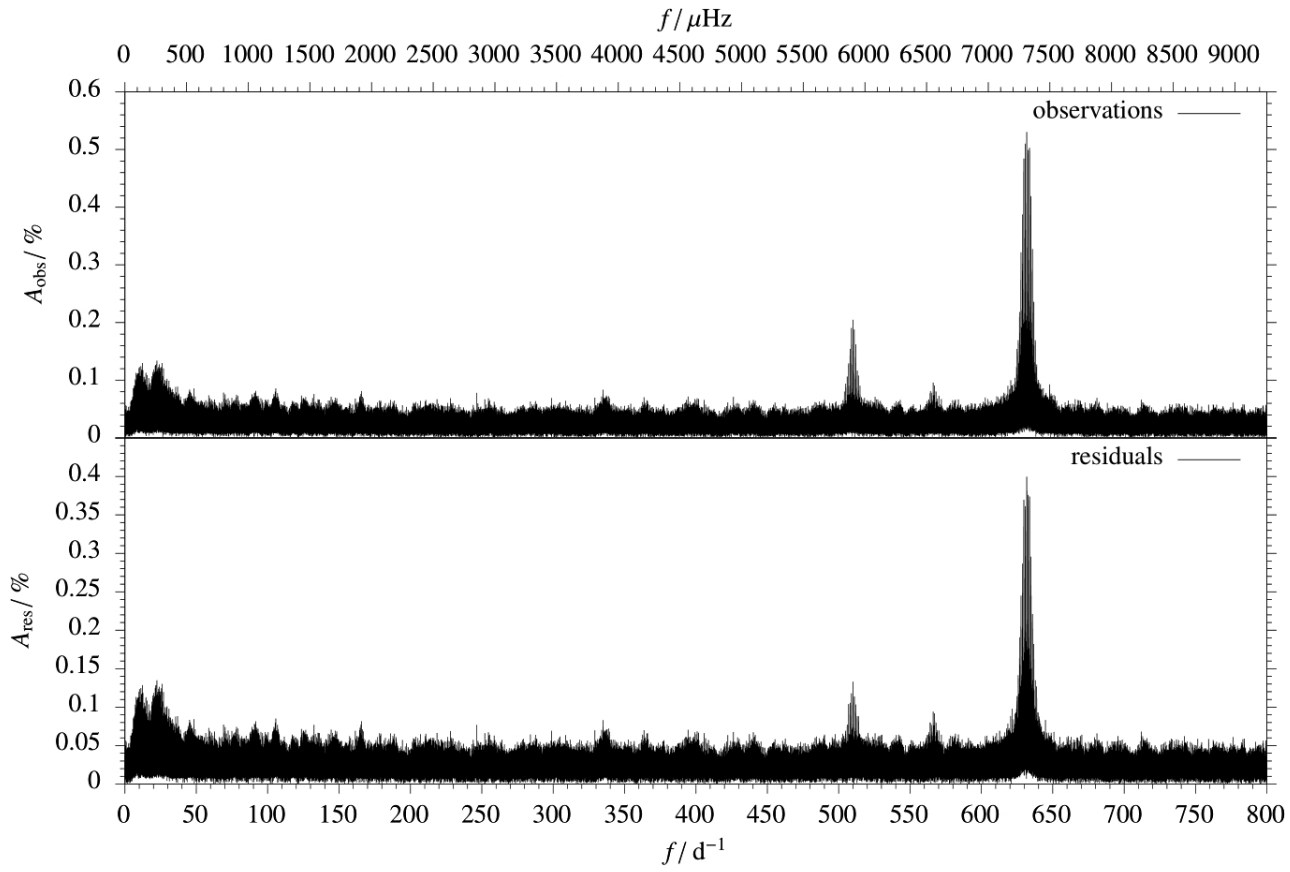

Fig. B.2. Same as Fig. B.1 but for V1636 Ori.

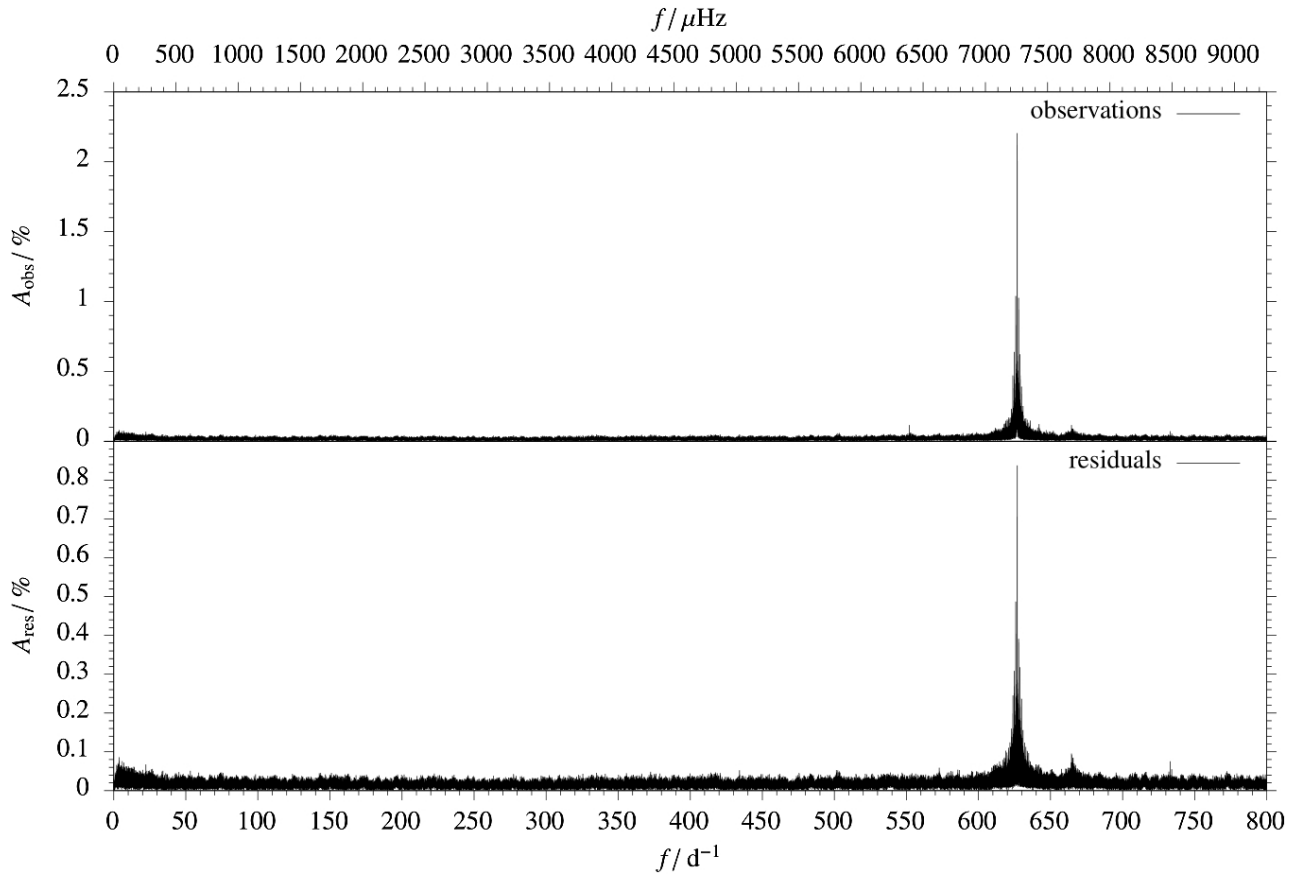

Fig. B.3. Same as Fig. B.1 but for QQ Vir.

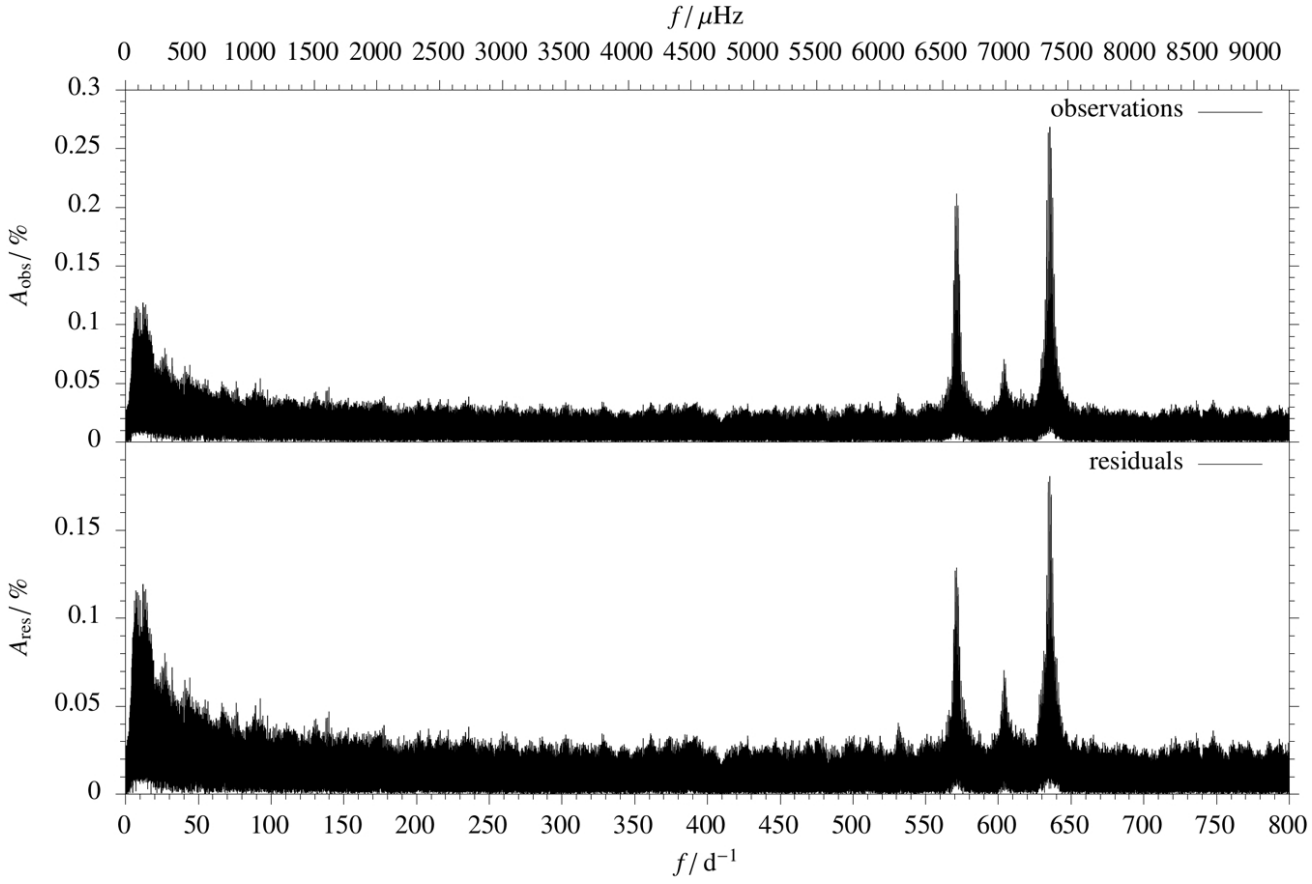

Fig. B.4. Same as Fig. B.1 but for V541 Hya.